ACS APPLIED MATERIALS & INTERFACES

Research Article

www.acsami.org

Ultrasensitive Bisphenol A Field-Effect Transistor Sensor Using an Aptamer-Modified Multichannel Carbon Nanofiber Transducer

Sung Gun Kim, Jun Seop Lee, Jaemoon Jun, Dong Hoon Shin, and Jyongsik Jang*

School of Chemical and Biological Engineering, College of Engineering, Seoul National University, 599 Gwanangno, Gwanakgu, Seoul 151-742 Korea

Supporting Information

ABSTRACT: Bisphenol A (BPA) is a known endocrine-disrupting compound (EDC) that has a structure similar to that of the hormone estrogen. Even low concentrations of BPA are able to bind estrogen receptors, thereby inducing severe diseases such as reproductive disorders, chronic diseases, and various types of cancer. Despite such serious effects, the use of BPA remains widespread. Therefore, monitoring of both dietary and nondietary exposure to BPA is important for human healthcare. Herein, we present a field-effect transistor (FET) sensor using aptamer-modified multichannel carbon nanofibers (MCNFs) to detect BPA. The MCNFs are fabricated via single-nozzle electrospinning of two immiscible polymer solutions followed by thermal treatment in an inert atmosphere. The MCNFs are then oxidized using a solution of HNO_3 and H_2SO_4 to introduce carboxyl groups on the surface of the fibers. The carboxyl-functionalized MCNFs (CMCNFs) are immobilized on an amine-functionalized electrode substrate by forming a covalent bond, and amine-functionalized BPA-binding aptamers are modified in the same manner on the CMCNFs. The resulting FET sensors exhibit a high sensitivity, as well as specificity toward BPA at an unprecedentedly low concentration of 1 fM. Furthermore, these sensors are stable and could be reused for repeated assays.

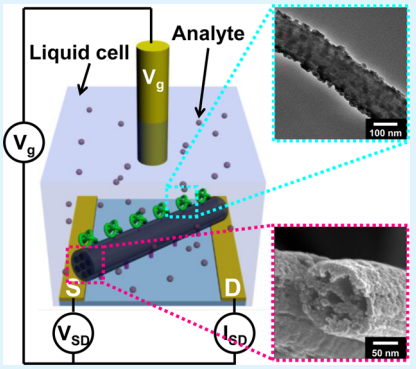

KEYWORDS: *carbon nanofiber, bisphenol A, aptamer, electrospinning, biosensor*

1. INTRODUCTION

In recent years, precise sensing platforms for the solution-phase detection of small molecules have become increasingly important for monitoring human diseases, food safety, and environmental contaminants. Bisphenol A (BPA) is a particularly important xenoestrogen, with a structure similar to that of the hormone estrogen, and is a known endocrine-disrupting compound (EDC).[1−4] Because of the structural similarity, even low concentrations (ca. 100 pM) of BPA are able to bind estrogen receptors (ERs), thereby inducing adverse changes such as reproductive disorders, chronic diseases, and various types of cancer, via both endocrine pathways[5−9] and genomic pathways.[10−14] Despite such serious effects on human health, the use of BPA still remains widespread for food storage and packaging which is of particular concern as BPA can readily migrate into food at high temperatures, as well as for thermal printing paper, medical materials, and adhesives.[15−17] In addition, since residual trace amounts of BPA are a potential endocrine disruptor, the maximum residue limit (MRL) for BPA in food or food packages was established at 0.6 μg/g by the European Union Legislation, and also the maximum acceptable dose and tolerable daily intake (TDI) for BPA were established by the European Food Safety Authority (EFSA).[18,19] Therefore, monitoring of both dietary and nondietary exposure to BPA is important for human healthcare.

Several approaches have been reported for detecting BPA at low concentrations.[20−24] High-performance liquid chromatography (HPLC) and gas chromatography coupled with mass spectrometry (GC/MS) are the most widely used methods to detect BPA. However, these techniques require large and expensive equipment which needs labor intensive processes, and the interpretation of data from these techniques is not always straightforward, as well. Immunoassays, using antibodies as biological recognition compounds, are another attractive simple method for screening small toxins such as BPA due to their low-cost aspect and high sensitivity. Nevertheless, in complex matrices including pH, salt concentrations, and other substances, the matrix effect associated with the quality of the antibody can cause nonspecific binding to the antibodies with structural analogues and then bring on degradation of the detection accuracy toward the antigen.

Aptamers are short, functional oligonucleotide sequences and have attracted considerable research interest for use as molecular recognition elements.[25−27] Owing to their high affinity and specificity toward certain ligands, the aptamers can be used to target various classes of molecules widely from whole cells to proteins and even in small molecules.[28−32] This allows one to identify various functional groups in the target molecular structure among structural analogues which have differences in some groups like methyl or hydroxyl groups. In

Received: November 18, 2015
Accepted: February 17, 2016

DOI: 10.1021/acsami.5b11159
ACS Appl. Mater. Interfaces XXXX, XXX, XXX−XXX

addition to the advantages of rapid synthesis, low cost, and facile modification, DNA aptamers have resistance to nuclease degradation, thermal stability, and reversible denaturation in comparison with RNA aptamers. Accordingly, these advantages mean that they have potential for reusable sensing applications. There have been a number of reports detailing the use of aptamers for the detection of biological molecules and small molecules, sometimes using nanomaterials to enhance sensitivity.[33−36]

Conductive nanomaterials including conducting polymers, nanostructured metal composite, and carbon nanomaterials have been studied because of their unique properties.[37−43] One-dimensional (1D) conductive nanomaterials have been shown to be particularly effective transducers due to their simple structure and fast directional charge transport characteristics.[44−48] Among the 1D materials, carbon nanomaterials are important for electrochemical and biological applications since their surface can be easily modified using a variety of covalent or π-stacking methods.[49,50] Especially, carbon nanofibers (CNFs) can be obtained via a simple electrospinning method, which has advantages relatively in terms of efficiency, cost, yield, and reproducibility. Electrospun CNFs are particularly attractive for sensing applications because their electrochemical properties and structures can be easily controlled by varying the process conditions, including temperature, spinning solution component, precursor composition, etc.[51−54] However, there remain some challenges such as the production of multidimensional nanofibers requires the optimization of a stable process for electrochemical and structural benefits.

Here, we report a field-effect transistor (FET) sensor for the detection of BPA based on multichannel carbon nanofibers (MCNFs) modified with BPA-binding aptamers. The MCNFs are fabricated via a facile single-nozzle coelectrospinning technique and are used as a conductive signal transducer. The multichannel structure enhances the specific surface area and thus improves the interactions between BPA molecules and the transducer. The MCNFs are located between the aptamers and the electrode substrate of the FET via covalent bonding, leading to a powerful affinity of the aptamer for the BPA molecules and consequently providing good electronic performance of the aptamer−FET sensor system. To the best of our knowledge, this represents the first demonstration of a FET-type aptamer sensor utilizing multichannel carbon nanofibers. The sensitivity was observed in various concentrations of BPA, giving an unprecedented detection limit of 1 fM. This result shows over ~10^3 times higher sensitivity compared with other BPA sensors such as those that are based on multiwalled carbon nanotubes.[55,56] In addition, this aptamer−FET sensor exhibited long-term stability and specificity toward BPA in the presence of structural analogues.

2. EXPERIMENTAL SECTION

2.1. Materials. Poly(acrylonitrile) (PAN), with a molecular weight of M_w = 150 000, and poly(methyl methacrylate) (PMMA), with a molecular weight of M_w = 350 000, were purchased from Aldrich. *N*,*N*-Dimethylformamide (DMF) (Aldrich) was used as the solvent for both the PAN and PMMA solutions. Bisphenol A (BPA) (i.e., 4,4′-(propane-2,2-diyl)diphenol) as well as the BPA structural analogues 4,4′-(butane-2,2-diyl) diphenol (Bisphenol B, BPB), 4,4-bis(4-hydroxyphenyl) valeric acid (VA), 4,4′-dihydroxybiphenyl (4,4′-biphenol, BP), and 4,4′-(hexafluoro-isopropylidene) diphenol (6F) were purchased from TCI. The BPA-binding aptamer was synthesized by Bioneer Co. (Daejeon, Korea). The sequence of the aptamer was 5′-NH_2-$(CH_2)_6$-CCG GTG GGT GGT CAG GTG GGA TAG CGT TCC GCG TAT GGC CCA GCG CAT CAC GGG TTC GCA CCA-3′, where A, T, G, and C represent adenine, thymine, guanine, and cytosine, respectively.[23,57] The aptamer stock solution was diluted with diethyl pyrocarbonate (DEPC) and water and stored in a freezer at −20 °C prior to use.

2.2. Fabrication of Carboxyl-Functionalized MCNFs. First, multichannel carbon nanofibers (MCNFs) were fabricated by electrospinning and subsequent heat treatment. PAN solutions were prepared by dissolving 1.0 g of PAN in 10 mL of DMF at 60 °C followed by vigorous stirring for 2 h. PMMA solutions were prepared in the same manner as PAN solutions. These polymer solutions were mixed in 1:1 ratios and stirred vigorously for 3 h. The resulting mixture was electrospun using a single 0.1 mm-diameter syringe nozzle with an applied voltage of 18 kV and a flow rate of 10 μL min^{-1}. The distance from the tip to the collector was fixed at 15 cm. The electrospun NFs were calcined at 400 °C for 2 h in air and then carbonized at 800 °C for 1 h in flowing argon.

Carboxyl-functionalized MCNFs (CMCNFs) were prepared via an oxidative treatment. MCNFs (250 mg) were added to 20 mL of a 3:1 volume mixture of 1 M sulfuric acid (H_2SO_4) and 1 M nitric acid (HNO_3) for a systematically varied period of time and diluted with distilled water. The mixed MCNFs solutions were purified by repeated centrifugation and multiple washing steps. The resulting CMCNF solutions were evaporated at 60 °C.

2.3. Fabrication of A-CMCNFs FET Sensor. To form aptamer-modified CMCNFs (A-CMCNFs) FET sensors, interdigitated array (IDA) electrodes were treated with 5 wt % aqueous aminosilane (i.e., 3-aminopropyltrimethoxysilane, APS) for 6 h to form amino groups on the electrode. The electrodes were then exposed to 40 μL of a mixture of 0.1 wt % aqueous CMCNFs solution and 1 wt % aqueous 4-(4,6-dimethoxy-1,3,5-triazin-2-yl)-4-methylmorpholinium chloride (DMT-MM, 40 μL) for 12 h. The resulting electrodes, with immobilized CMCNFs, were rinsed with distilled water to remove extra residues including DMT-MM and unbound CMCNFs. A coupling reaction to attach the BPA-binding aptamer to the CMCNF surface was then carried out using a mixture of the binding aptamer and 1 wt % aqueous DMT-MM (40 μL) for 12 h. The A-CMCNFs immobilized electrodes were then rinsed with distilled water repeatedly and dried at room temperature.

2.4. Extraction of the Actual Bisphenol A Samples. A polycarbonate (PC) bottle and thermal printing paper were prepared to extract BPA. The PC bottle filled with distilled water was sonicated and then immersed in an oil bath at 70 °C for 1 h. After filtration, the liquid was collected. The thermal printing paper (10 mg) was immersed in 10 mL of absolute ethanol at 70 °C for 1 h. After filtration, extracts were diluted 1:1000 in distilled water.

2.5. Electrical Measurements of the A-CMCNFs FET Sensor. All electrical measurements were carried out using a Keithley 2612A source meter and a probe station (MS TECH, model 4000). A 300 μL chamber was used for solution-based measurements. The measured current was normalized as follows:

$$\left[\frac{\Delta I}{I_0}\right]_{SD}(\%) = \frac{(I - I_0)}{I_0} \times 100$$

where I_0 is the initial measured current and I is the time-varying measured current. The A-CMCNFs FET sensors were carried out with the following recycling process: (i) immobilizing BPA-binding aptamers on IDA electrodes as mentioned above, (ii) injecting BPA molecule into the A-CMCNFs FET sensor, and (iii) washing with 10% sodium chloride solution and air-drying.

2.6. Instruments. TEM micrographs were obtained using JEOL JEM-200CX microscopes. A JEOL 6700 was used to obtain FE-SEM micrographs. IR spectra were recorded using an ATR-IR spectrometer (Frontier, PerkinElmer), and XPS spectra were recorded on an Axis-His system (KRATOS).

DOI: 10.1021/acsami.5b11159
ACS Appl. Mater. Interfaces XXXX, XXX, XXX−XXX

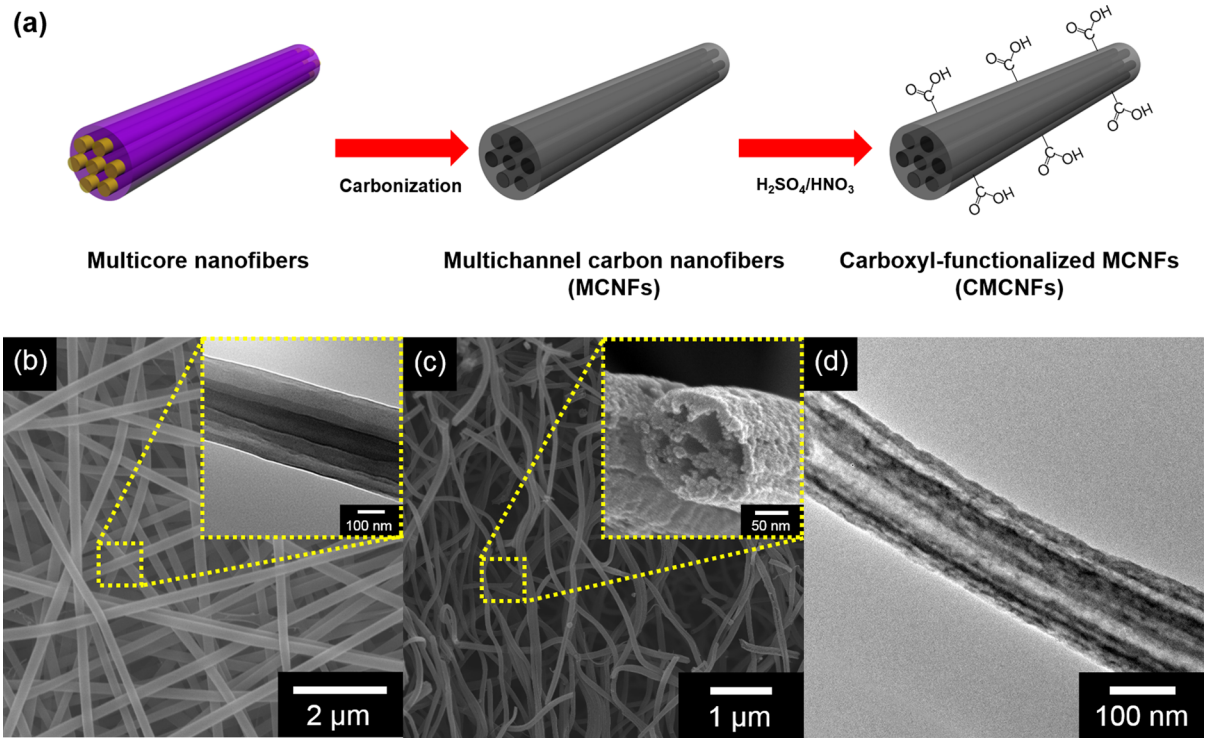

Figure 1. (a) Schematic diagram of carboxyl-functionalized multichannel carbon nanofibers (CMCNFs); (b) FE-SEM and TEM micrographs show the multicore nanofibers; (c) FE-SEM micrographs of the multichannel carbon nanofibers (MCNFs). The inset showing a magnified cross-section of a MCNF. (d) A TEM micrograph of a CMCNF.

3. RESULTS AND DISCUSSION

3.1. Fabrication of CMCNFs. Figure 1a illustrates an overview of the fabrication process of carboxyl-functionalized multichannel carbon nanofibers (CMCNFs) via single-nozzle coelectrospinning and oxidative treatment. First, a 1:1 (by volume) solution of poly(acrylonitrile) (PAN) and poly(methyl methacrylate) (PMMA) was prepared, which resulted in a phase-separated polymer blend because of the interfacial tension, viscosity, and elasticity of the polymers (see inset of Figure S1). In this phase-separated blend, the high surface tension of the PMMA resulted in the formation of discontinuous droplets, whereas the more viscous PAN occupied the continuous phase of the solution. During coelectrospinning of this mixed solution, the discrete PMMA droplets elongated along the inside of the PAN shell due to the stretching force of the applied voltage, leading to the formation of multicore nanofibers (Figures S1 and 1b). These multicore nanofibers were uniform with a diameter of ca. 300 nm. The phase-separated polymer nanofibers were then stabilized at 400 °C for 2 h and carbonized at 800 °C for 1 h in a flowing argon atmosphere. Multichannel carbon nanofibers (MCNFs) were formed during this heat treatment step. The continuous PAN phase (shell) was transformed into carbon while the inner elongated PMMA phase (cores) decomposed, resulting in the formation of an internal multichannel (Figures 1c and S2a).[54] Owing to the elimination of PMMA from within the fibers, the multicore nanofibers constricted over the heating process. Eventually, the diameter of the resulting MCNFs was ca. 150 nm with ca. 20 nm-diameter internal channels. The following oxidation procedure was carried out to functionalize the surface of the MCNFs. The MCNFs were treated with a mixture of 1 M sulfuric acid and 1 M nitric acid (3:1 volume ratio) at room temperature, where the reaction time was systematically controlled, and the resulting MCNFs were washed with distilled water and dried at 60 °C. As a consequence, CMCNFs were well-fabricated, exhibiting well-defined structures without collapse of the channels, as suggested in Figure 1d. In addition, due to the control of oxidation time, the quantity of the carboxyl-functional groups were optimized. If the oxidation time was longer than 12 h, there were overall morphology changes: the multichannel structure of the MCNFs was collapsed, and the outer shells of the fibers were combined with each other (Figure S3).

Fourier-transform infrared (FTIR) spectra of the CMCNFs are presented in Figure 2. Functionalization of the surface of the MCNFs is evidenced by peaks associated with oxygen, including the C═O stretching peak at 1720 cm^{-1}, the stretching vibration and deformation peaks of −OH groups at 3430 and 1400 cm^{-1}, and the stretching vibration peaks of

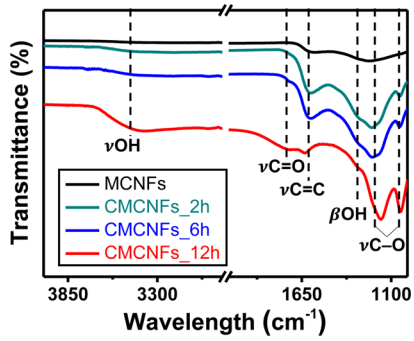

Figure 2. FTIR spectra of MCNFs and the CMCNFs formed with oxidation times of 2, 6, and 12 h (CMCNFs_2h, CMCNFs_6h, and CMCNFs_12h).

DOI: 10.1021/acsami.5b11159
ACS Appl. Mater. Interfaces XXXX, XXX, XXX−XXX

C−O bonds (including those in phenol groups) at 1080 and 1230 cm^{-1}. The peak at 1590 cm^{-1} corresponds to structural lattice vibrations of the CNFs and indicates that the structure of the CMCNFs remained intact after acid treatment. The increase in the intensity of the characteristic peaks at 1230, 1720, and 3430 cm^{-1} suggests that carboxyl groups were properly formed on the surface of the MCNFs as the acid treatment time.

The chemical composition of these CMCNFs was also investigated by X-ray photoelectron spectroscopy (XPS). Figure 3 displays high-resolution XPS spectra for the C (1s)

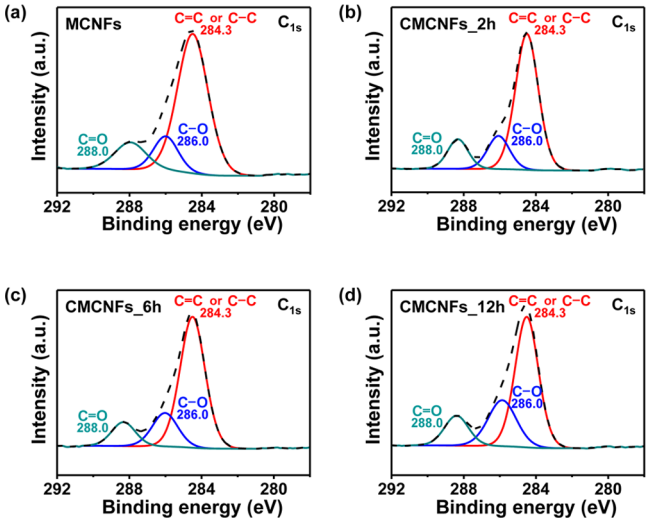

Figure 3. XPS C (1s) survey spectra of MCNFs and the CMCNFs formed with oxidation times of 2, 6, and 12 h. (a) MCNFs, (b) CMCNFs_2h, (c) CMCNFs_6h, and (d) CMCNFs_12h.

region around 284.5 eV; these peaks were deconvolved into component peaks of C═C and C−C (284.3 eV) in the aromatic rings, C−O (286.0 eV) in the epoxy and hydroxyl groups, and C═O (288.0 eV) derived from carbonyl and carboxyl groups. An increase in peak intensity associated with carboxyl groups was observed by comparing the intensity of peaks referring to oxygen-related functional groups. This demonstrated that the intensity ratios I_{C-O} and $I_{C=O}$ increased gradually as oxidation time increased, according to an increase in the quantity of oxygen in the CMCNFs. These spectral investigations indicate that carboxyl groups were well functionalized on the MCNFs through oxidative treatment.

3.2. Fabrication of A-CMCNFs FET Sensor Electrode. To fabricate a sensitive FET sensor electrode, the transducer CMCNFs were located between the binding aptamers and the electrode via covalent bonding of functional groups, respectively. Figure 4 depicts a schematic illustration detailing the formation of aptamer-modified CMCNFs (A-CMCNFs) on the electrode substrate. An interdigitated array (IDA) consisting of two sets of 25 interdigitated gold electrodes was used as the substrate for immobilization. The surface of the IDA substrate was modified with amine group (—NH_2) using 3-aminopropyltrimethoxysilane (APS), and the CMCNFs were fixed to the electrode substrate via coupling reactions between the carboxyl group (—COOH) of the CMCNFs and the —NH_2 group of the APS involving the condensation agent 4-(4,6-dimethoxy-1,3,5-triazin-2-yl)-4-methylmorpholinium chloride (DMT-MM). The carboxyl groups of the CMCMFs enabled the formation of covalent bonds with the substrate, as well as with the binding aptamers. To achieve covalent binding of the aptamers onto the carboxyl group, the 5′-end of the BPA-binding aptamers was decorated with a primary amino group, which was separated from the 5′-end base via a six-carbon spacer to reduce steric interaction between the amino group and the oligomer. Subsequently, via identical coupling reactions with DMT-MM, the CMCNFs were conjugated to the BPA-binding aptamers without binding to the substrate. In particular, as exhibited in Figures S2c and S4, the specific surface area increased due to the formation of internal channels, which increased the quantity of immobilized BPA-binding aptamers. Moreover, there were well-developed 5−10 nm of mesopores which were pathways of the residual gas during thermal decomposition process (see Figure S4b). Especially, because the size of the binding aptamers was approximately ∼2 nm, they could pass through the 5−10 nm-diameter mesopores as well as 20 nm-diameter internal channels of the fibers.[58] In this manner, A-CMCNFs were immobilized onto the sensor electrode substrate.

3.3. Characterization of A-CMCNFs FET Sensors. Figure 5a illustrates the configuration of the FET sensor, which included an electrolyte liquid−ion gate dielectric and the A-CMCNFs as a conductive channel. Figure 5b indicates the current−voltage (I−V) characteristics of the A-CMCNFs. We found a linear dependence of the current on the voltage from −0.1 to 0.1 V. This finding contrasts with the nonlinear characteristics exhibited by devices that contain Schottky barriers with electrical poor contact at the electrode. Namely, the conductive A-CMCNFs formed Ohmic contacts with the electrodes. The dV/dI value increased with increasing acid treatment time, due to the increase in the number of carboxyl groups. However, the order of magnitude of dV/dI did not change, and linear Ohmic properties were maintained after aptamer immobilization. These results suggest that covalent immobilization of the aptamers was successful and that the electrical contacts were reproducible. Figure 5c means the source−drain current, I_{SD}, as a function of the source−drain bias, V_{SD}, with various gate biases, V_g, for a liquid−ion-gated FET device formed with an acid treatment time of 12 h. Compared with conventional back-gating, liquid−ion gating enabled intimate contact with the CNFs, which increased transconductance.[59] The I−V measurements show that I_{SD} increased (became more negative) as V_g decreased from +0.8 to −1.0 V, indicating p-type behavior (i.e., hole transport). We believe that varying V_g altered the oxidation level of the CMCNFs and hence the charge carrier distribution.

3.4. Real-Time Responses of A-CMCNFs FET Sensors. To evaluate the sensing characteristics of the liquid−ion-gated A-CMCNFs FET sensors, changes in I_{SD} were observed in real time, with V_g = 50 mV and V_{SD} = 50 mV, during the introduction of solutions containing various concentrations of BPA. Figure 6a exhibited the real-time response of sensors formed after oxidization via acid treatment for 2, 6, and 12 h. Following the injection of BPA, I_{SD} decreased rapidly within ca. 1 s and saturated. The decrease in I_{SD} was caused by interactions between BPA and the aptamers during the formation of aptamer−BPA complexes.[11,36,60] The immobilized aptamers were negatively charged, and BPA binds specifically to the A-CMCNFs due to the intermolecular interactions, such as the stacking of aromatic rings, electrostatic and van der Waals interactions, or hydrogen bonding with target compounds.[61] When the aptamer−BPA complex forms, there may be some structural rearrangement of the aptamer strand, leading to an

DOI: 10.1021/acsami.5b11159
ACS Appl. Mater. Interfaces XXXX, XXX, XXX−XXX

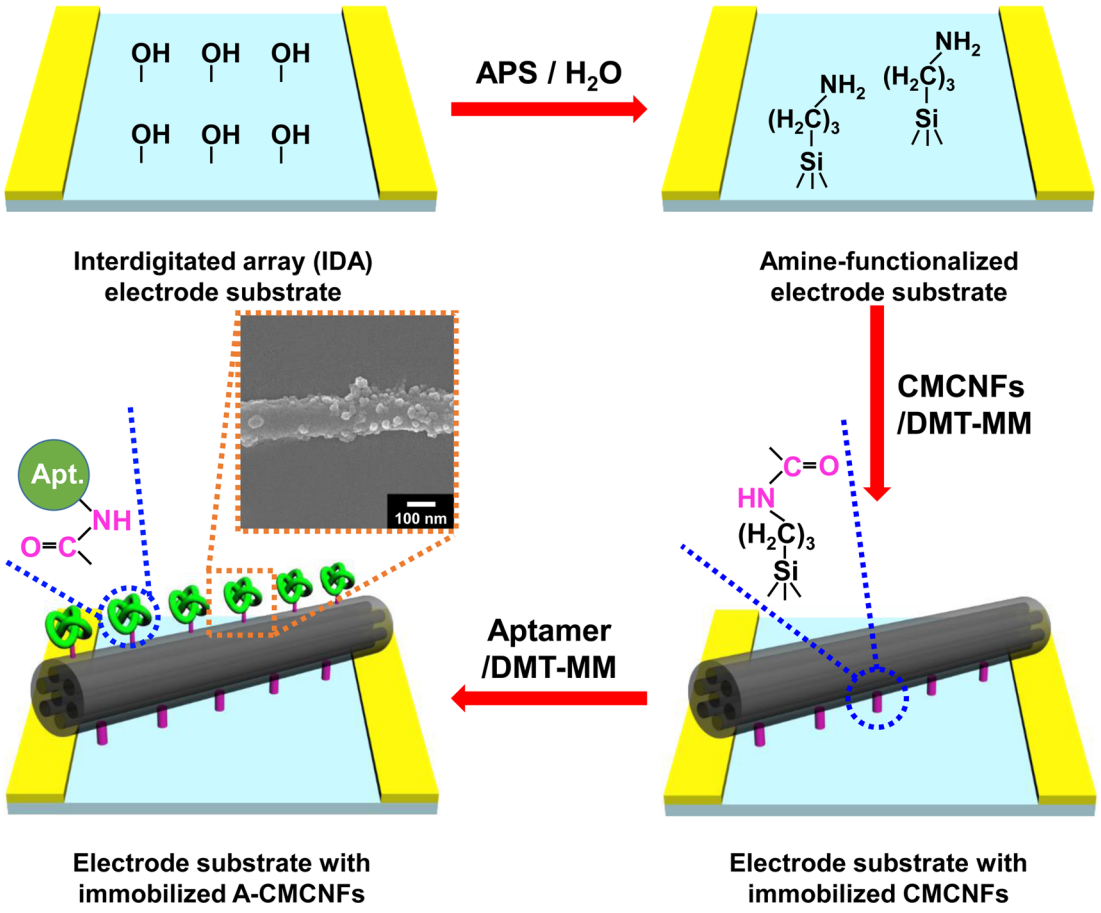

Figure 4. Schematic diagram showing the immobilization of aptamer-modified CMCNFs (A-CMCNFs) on the electrode (Apt.: aptamer).

influence of the negative charge density at the surface of the A-CMCNFs. This induces the screening effect on the negative charge of the aptamers and also changes the charge-transport properties of the A-CMCNFs that may reduce the hopping rate of charge carriers, resulting in a decrease in I_{SD}.

As shown in Figure 6a, the sensitivity of the A-CMCNFs FET sensors increased with acid treatment time. The greater the degree of oxidization of the MCNFs, the denser is the chemical functionality; in other words, the amount of carboxylic acid groups and immobilized aptamers increased as the acid treatment time increased. For this reason, the A-CMCNFs oxidized for 12 h were able to detect BPA rapidly and remarkably down to 1 fM (signal-to-noise ratio ≥3.0), considering other various sensors developed for the analysis of BPA (Table S1). Figure 6b exhibits the sensitivity, S, of the A-CMCNFs as a function of BPA concentration. The sensitivity was determined from the normalized change in the current (i.e., the saturation level of $[\Delta I/I_0]_{SD} \times 100$ measured after exposure to the analyte for 10 s). Over a large concentration range of 10^0–10^4 fM, the sensitivity of the A-CMCNF sensor to BPA increased linearly with concentration. The linear equations were as follows:

$$S\,(\%) = 2.8597 \log C + 1.0768$$

$$S\,(\%) = 2.7794 \log C - 1.6748$$

$$S\,(\%) = 2.2235 \log C - 3.4251$$

where C is BPA concentration (fM). Owing to the enhancement of the functional sites for binding BPA with increasing acid treatment time, the sensitivity of the A-CMCNF sensor treated for 12 h was the highest.

In Figure 7, The specificity of the A-CMCNFs FET sensors was examined using the following BPA structural analogues: 4,4′-(butane-2,2-diyl) diphenol (Bisphenol B, BPB), 4,4-bis(4-hydroxyphenyl) valeric acid (VA), 4,4′-(hexafluoroisopropylidene) diphenol (6F), and 4,4′-dihydroxybiphenyl (4,4′-biphenol, BP) (see molecular diagrams in Figure S5). The A-CMCNFs FET sensor exhibited insignificant changes in I_{SD} following exposure to 1 μM solutions of the structural analogues (i.e., nontarget molecules). However, a much larger change in the signal occurred immediately following exposure to a 1 fM solution of BPA, as described in Figure 7a. In addition, 1 μM solutions of mixed structural analogues were prepared with and without 1 fM of BPA and were added consecutively and individually to further investigate the specificity. As presented in Figure 7b, there was a significant change in I_{SD} following the introduction of mixtures containing BPA, relative to that experienced without BPA. This demonstrated that the A-CMCNFs FET sensor was highly specific for BPA.

On the basis of above results of the real-time response, the real samples were prepared to make sure of the sensing performance of the A-CMCNFs FET sensor to BPA. Polycarbonate (PC) bottles and thermal printing paper are typical examples that leach out BPA in hot environments.[62,63] Real examples 1 and 2 were extracted from a PC bottle with hot water and from thermal printing paper immersed in hot ethanol, respectively. Figure 7c shows the real-time response of

DOI: 10.1021/acsami.5b11159
ACS Appl. Mater. Interfaces XXXX, XXX, XXX−XXX

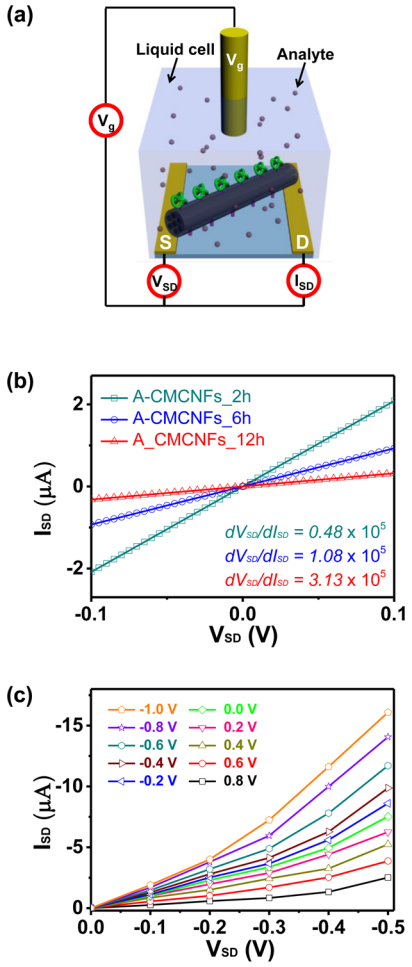

Figure 5. (a) Schematic diagram showing the operating principle of the liquid–ion-gated FET sensor with A-CMCNFs. (b) Source–drain current–voltage (I_{SD}–V_{SD}) curves of sensors formed using A-CMCNFs, shown for oxidation times of 2, 6, and 12 h following the introduction of BPA-binding aptamers. (c) I_{SD}–V_{SD} characteristics of A-CMCNFs FET electrodes, shown for gate voltages of −1.0 V ≤ V_g ≤ + 0.8 V in steps of 0.2 V with a V_{SD} scan rate of 10 mV s^{-1}.

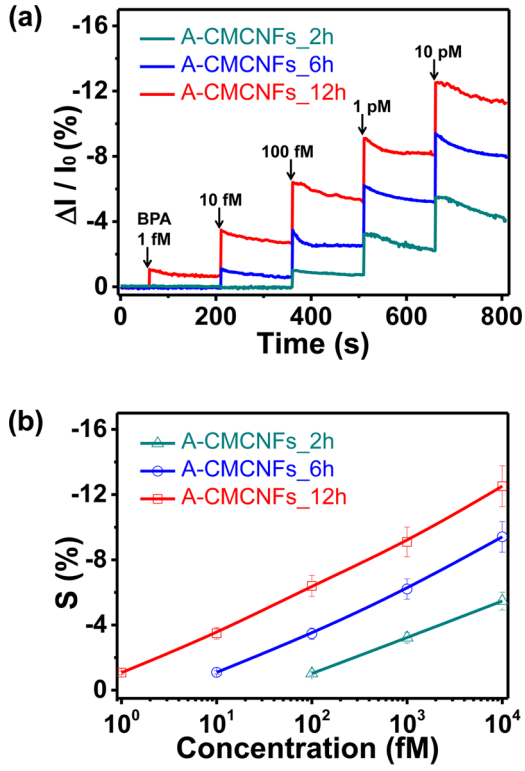

Figure 6. (a) Real-time response of the normalized current (i.e., $[\Delta I/I_0]_{SD}$ × 100) of A-CMCNFs FET sensors formed with various oxidation times. (b) Calibration curves of FET sensors formed with various acid treatment times as a function of BPA concentration. Here, *S* denotes the normalized current following 10 s of exposure to the BPA solution. Dark cyan, blue, and red correspond to oxidation times of 2, 6, and 12 h, respectively. The gate bias was V_g = 50 mV, and the source–drain bias was V_{SD} = 50 mV.

the A-CMCNFs FET sensor to actual BPA extracted samples. Owing to the high sensitivity and specificity of the aptasensor, the current signal strikingly changed when the sensor was exposed in serial order of the real samples. Consequently, results presented in Figure 7 display that the A-CMCNFs FET sensor is able to discriminate BPA in real samples and it can be applied to further applications of BPA determinations.

Figure 8 depicts the stability of the sensor, on the basis of the responses of various A-CMCNFs FET sensors over a period of several weeks. The A-CMCNFs FET sensors were maintained in a closed receptacle at 25 °C in dry conditions for 4 weeks. In addition, the signal stability of A-CMCNFs FET sensors with a 1 pM solution of BPA was observed over a period of 7 days. Prior to sequentially dropping target molecules onto the FET sensors, the sensors were washed with PBS solution and rinsed with distilled water to remove salt residues. After 4 weeks, the sensitivity decreased by 87%, 89%, and 90% for sensors formed with 2, 6, and 12 h acid treatments, respectively. This decrease in sensitivity is attributed to damage to the sensor array or degradation of the binding aptamers. However, the sensing performance was maintained during repeated response tests, and the decrease in sensitivity over time was not large. Judging from these results, the stability is attributed to the covalent bonding between the binding aptamers, the CMCNFs, and the electrode substrate. Besides, the binding aptamer itself has its own endurance in the external environment. From this point of view, the A-CMCNFs FET sensors are stable and can be reused for repeated assays.

Compared to other several biosensors to detect BPA, the A-CMCNFs FET sensors have more superiority in various aspects.[64−69] The first is an unprecedented limit of detection (LOD) of 1 fM (1 × 10^{-15} M) for detecting BPA which is higher than other BPA biosensors including aptamer-based sensors. In addition to the sensitivity, the A-CMCNFs FET sensor responds directly in seconds when exposed to BPA, whereas other methods such as the electrochemical or catalytic process need time. In terms of the cost, the aptasensor utilizes multichannel structured carbon nanofibers which are cheap and facile to fabricate through the electrospinning method. The structural benefit provides enhanced reaction cites to detect BPA at extremely low levels. Considering the above features, the FET sensor utilizing A-CMCNFs as a transducer has predominant advantages.

4. CONCLUSIONS

We successfully fabricated liquid–ion-gated FET sensors based on the A-CMCNFs to detect BPA. The fibers were formed using single-nozzle electrospinning followed by acid treatment to immobilize the aptamers, which enabled control over the degree of aptamer functionalization. The internal multichannel

DOI: 10.1021/acsami.5b11159
ACS Appl. Mater. Interfaces XXXX, XXX, XXX−XXX

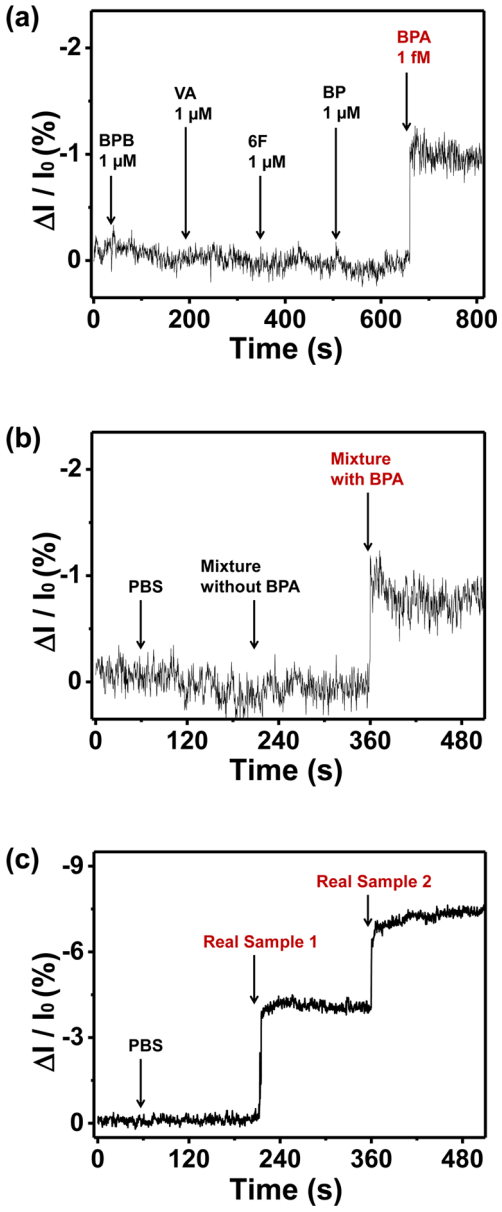

Figure 7. Real-time response of A-CMCNFs FET sensor (a) to BPA structural analogues 4,4′-(butane-2,2-diyl) diphenol (Bisphenol B, BPB), 4,4-bis(4-hydroxyphenyl) valeric acid (VA), 4,4′-(hexafluoroisopropylidene) diphenol (6F), and 4,4′-dihydroxybiphenyl (4,4′-biphenol, BP), (b) to various analytes before and after being mixed with BPA, and (c) to actual BPA extracted samples (real sample 1: polycarbonate (PC) bottle; sample 2: thermal printing paper). The gate bias was V_g = 50 mV, and the source−drain bias was V_{SD} = 50 mV.

structure resulted in a large specific surface area and hence a large quantity of conjugated aptamers. The optimized degree of functionalization and large specific surface area resulted in high sensitivity and specificity for BPA, much higher than that of other BPA sensors. Owing to the immobilization of the aptamers via covalent bonding, the A-CMCNFs FET sensors were stable and could be reused over a period of 4 weeks. Considering these advantageous results, the A-CMCNFs FET sensors enabled the highly sensitive and specific detection of BPA at concentrations unprecedentedly down to 1 fM, as well as good stability.

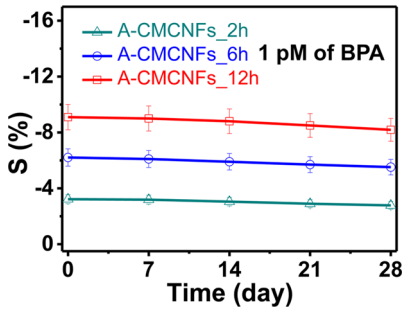

Figure 8. Stability of the A-CMCNFs FET sensors measured over 4 weeks with intervals of 7 days. Dark cyan, blue, and red correspond to oxidation times of 2, 6, and 12 h, respectively.

■ ASSOCIATED CONTENT

Supporting Information

The Supporting Information is available free of charge on the ACS Publications website at DOI: 10.1021/acsami.5b11159.

(1) Schematic diagram of the single-nozzle coelectrospinning method, (2) TEM micrographs of various MCNFs, (3) FE-SEM micrographs of the overoxidized MCNFs, (4) Brunauer−Emmett−Teller (BET) and Barrett−Joyner−Halenda (BJA) analysis, (5) performances of various sensors developed for the analysis of BPA, and (6) molecular diagrams of the structural analogues of BPA. (PDF)

■ AUTHOR INFORMATION

Corresponding Author

*Tel.: 82-2-880-7069. Fax: 82-2-888-7295. E-mail: jsjang@plaza.snu.ac.kr.

Notes

The authors declare no competing financial interest.

■ ACKNOWLEDGMENTS

This research was supported by the National Research Foundation of Korea (NRF) grant funded by the Korean government (MEST) (no. 2011-0017125)

■ REFERENCES

(1) Den Hond, E.; Tournaye, H.; De Sutter, P.; Ombelet, W.; Baeyens, W.; Covaci, A.; Cox, B.; Nawrot, T. S.; Van Larebeke, N.; D'Hooghe, T. Human Exposure to Endocrine Disrupting Chemicals and Fertility: A Case-Control Study in Male Subfertility Patients. *Environ. Int.* **2015**, *84*, 154−160.

(2) Schneider, J. E.; Brozek, J. M.; Keen-Rhinehart, E. Our Stolen Figures: The Interface of Sexual Differentiation, Endocrine Disruptors, Maternal Programming, and Energy Balance. *Horm. Behav.* **2014**, *66* (1), 104−119.

(3) Futran Fuhrman, V.; Tal, A.; Arnon, S. Why Endocrine Disrupting Chemicals (EDCs) Challenge Traditional Risk Assessment and How To Respond. *J. Hazard. Mater.* **2015**, *286*, 589−611.

(4) Rappaport, S. M.; Smith, M. T. Environment and Disease Risks. *Science* **2010**, *330* (6003), 460−461.

(5) Rosenfeld, C. S. Bisphenol A and Phthalate Endocrine Disruption of Parental and Social Behaviors. *Front. Neurosci.* **2015**, *9*, 57.

(6) Huo, X.; Chen, D.; He, Y.; Zhu, W.; Zhou, W.; Zhang, J. Bisphenol-A and Female Infertility: A Possible Role of Gene-Environment Interactions. *Int. J. Environ. Res. Public Health* **2015**, *12* (9), 11101−11116.

(7) Duntas, L. H. Chemical Contamination and the Thyroid. *Endocrine* **2015**, *48* (1), 53−64.

DOI: 10.1021/acsami.5b11159
ACS Appl. Mater. Interfaces XXXX, XXX, XXX−XXX

(8) Mustieles, V.; Perez-Lobato, R.; Olea, N.; Fernandez, M. F. Bisphenol A: Human Exposure and Neurobehavior. *NeuroToxicology* **2015**, *49*, 174−184.
(9) Vandenberg, L. N.; Hauser, R.; Marcus, M.; Olea, N.; Welshons, W. V. Human Exposure to Bisphenol A (BPA). *Reprod. Toxicol.* **2007**, *24* (2), 139−177.
(10) Thompson, P. A.; Khatami, M.; Baglole, C. J.; Sun, J.; Harris, S.; Moon, E. Y.; Al-Mulla, F.; Al-Temaimi, R.; Brown, D.; Colacci, A.; Mondello, C.; Raju, J.; Ryan, E.; Woodrick, J.; Scovassi, I.; Singh, N.; Vaccari, M.; Roy, R.; Forte, S.; Memeo, L.; Salem, H. K.; Amedei, A.; Hamid, R. A.; Lowe, L.; Guarnieri, T.; Bisson, W. H. Environmental Immune Disruptors, Inflammation and Cancer Risk. *Carcinogenesis* **2015**, *36*, S232−S253.
(11) Rezg, R.; El-Fazaa, S.; Gharbi, N.; Mornagui, B. Bisphenol A and Human Chronic Diseases: Current Evidences, Possible Mechanisms, and Future Perspectives. *Environ. Int.* **2014**, *64*, 83−90.
(12) Rancière, F.; Lyons, J. G.; Loh, V. H. Y.; Botton, J.; Galloway, T.; Wang, T.; Shaw, J. E.; Magliano, D. J. Bisphenol A and the Risk of Cardiometabolic Disorders: A Systematic Review with Meta-Analysis of the Epidemiological Evidence. *Environ. Health (London, U. K.)* **2015**, *14* (1), 46.
(13) Oppeneer, S. J.; Robien, K. Bisphenol A Exposure and Associations with Obesity among Adults: A Critical Review. *Public Health Nutr.* **2015**, *18* (10), 1847−1863.
(14) Mirmira, P.; Evans-Molina, C. Bisphenol A, Obesity, and Type 2 Diabetes Mellitus: Genuine Concern or Unnecessary Preoccupation? *Transl. Res.* **2014**, *164* (1), 13−21.
(15) Geens, T.; Aerts, D.; Berthot, C.; Bourguignon, J. P.; Goeyens, L.; Lecomte, P.; Maghuin-Rogister, G.; Pironnet, A. M.; Pussemier, L.; Scippo, M. L.; Van Loco, J.; Covaci, A. A Review of Dietary and Non-Dietary Exposure to Bisphenol-A. *Food Chem. Toxicol.* **2012**, *50* (10), 3725−3740.
(16) Mathieu-Denoncourt, J.; Wallace, S. J.; de Solla, S. R.; Langlois, V. S. Plasticizer Endocrine Disruption: Highlighting Developmental and Reproductive Effects in Mammals and Non-Mammalian Aquatic Species. *Gen. Comp. Endocrinol.* **2015**, *219*, 74−88.
(17) Rubin, B. S. Bisphenol A: An Endocrine Disruptor with Widespread Exposure and Multiple Effects. *J. Steroid Biochem. Mol. Biol.* **2011**, *127* (1−2), 27−34.
(18) EU (European Union). Commission Directive 2004/19/EC of 1 March 2004 Amending Directive 2002/72/EC Relating to Plastic Materials and Articles Intended to Come into Contact with Foodstuffs. *Off. J. Eur. Communities* **2004**, *L71*, 8−21.
(19) European Food Safety Authority (EFSA). Opinion of the Scientific Panel on Food Additives, Flavourings, Processing Aids and Materials in Contact with Food on a request from the Commission related to 2,2-BIS(4-HYDROXYPHENYL)PROPANE (Bisphenol A). *EFSA J.* **2006**, *428*, 1−75.
(20) Li, X.; Franke, A. A. Improvement of Bisphenol A Quantitation from Urine by LCMS. *Anal. Bioanal. Chem.* **2015**, *407* (13), 3869−3874.
(21) Ballesteros-Gomez, A.; Rubio, S.; Perez-Bendito, D. Analytical Methods for the Determination of Bisphenol A in Food. *J. Chromatogr. A* **2009**, *1216* (3), 449−469.
(22) Capriotti, A. L.; Cavaliere, C.; Colapicchioni, V.; Piovesana, S.; Samperi, R.; Laganà, A. Analytical Strategies Based on Chromatography−Mass Spectrometry for the Determination of Estrogen-Mimicking Compounds in Food. *J. Chromatogr. A* **2013**, *1313*, 62−77.
(23) Jo, M.; Ahn, J. Y.; Lee, J.; Lee, S.; Hong, S. W.; Yoo, J. W.; Kang, J.; Dua, P.; Lee, D. K.; Hong, S.; Kim, S. Development of Single-Stranded DNA Aptamers for Specific Bisphenol A Detection. *Oligonucleotides* **2011**, *21* (2), 85−91.
(24) Asimakopoulos, A. G.; Thomaidis, N. S.; Koupparis, M. A. Recent Trends in Biomonitoring of Bisphenol A, 4-t-Octylphenol, and 4-Nonylphenol. *Toxicol. Lett.* **2012**, *210* (2), 141−154.
(25) Liu, J.; Cao, Z.; Lu, Y. Functional Nucleic Acid Sensors. *Chem. Rev.* **2009**, *109* (5), 1948−1998.
(26) Lao, Y. H.; Phua, K. K. L.; Leong, K. W. Aptamer Nanomedicine for Cancer Therapeutics: Barriers and Potential for Translation. *ACS Nano* **2015**, *9* (3), 2235−2254.
(27) Song, J.; Lau, P. S.; Liu, M.; Shuang, S.; Dong, C.; Li, Y. A General Strategy To Create RNA Aptamer Sensors Using Regulated Graphene Oxide Adsorption. *ACS Appl. Mater. Interfaces* **2014**, *6* (24), 21806−21812.
(28) Amaya-González, S.; de-los-Santos-Álvarez, N.; Miranda-Ordieres, A.; Lobo-Castañón, M. Aptamer-Based Analysis: A Promising Alternative for Food Safety Control. *Sensors* **2013**, *13* (12), 16292.
(29) Hong, K. L.; Sooter, L. J. Single-Stranded DNA Aptamers against Pathogens and Toxins: Identification and Biosensing Applications. *BioMed Res. Int.* **2015**, *2015*, 31.
(30) Oh, S. S.; Lee, B. F.; Leibfarth, F. A.; Eisenstein, M.; Robb, M. J.; Lynd, N. A.; Hawker, C. J.; Soh, H. T. Synthetic Aptamer-Polymer Hybrid Constructs for Programmed Drug Delivery into Specific Target Cells. *J. Am. Chem. Soc.* **2014**, *136* (42), 15010−15015.
(31) Vinkenborg, J. L.; Karnowski, N.; Famulok, M. Aptamers for Allosteric Regulation. *Nat. Chem. Biol.* **2011**, *7* (8), 519−527.
(32) Oliveira, O. N.; Iost, R. M.; Siqueira, J. R.; Crespilho, F. N.; Caseli, L. Nanomaterials for Diagnosis: Challenges and Applications in Smart Devices Based on Molecular Recognition. *ACS Appl. Mater. Interfaces* **2014**, *6* (17), 14745−14766.
(33) Shiao, Y. S.; Chiu, H. H.; Wu, P. H.; Huang, Y. F. Aptamer-Functionalized Gold Nanoparticles as Photoresponsive Nanoplatform for Co-Drug Delivery. *ACS Appl. Mater. Interfaces* **2014**, *6* (24), 21832−21841.
(34) Wang, Z.; Yang, Y.; Xu, Z.; Wang, Y.; Zhang, W.; Shi, P. Interrogation of Cellular Innate Immunity by Diamond-Nanoneedle-Assisted Intracellular Molecular Fishing. *Nano Lett.* **2015**, *15* (10), 7058−7063.
(35) Kwon, O. S.; Park, S. J.; Jang, J. A High-Performance VEGF Aptamer Functionalized Polypyrrole Nanotube Biosensor. *Biomaterials* **2010**, *31* (17), 4740−4747.
(36) Yoon, H.; Kim, J. H.; Lee, N.; Kim, B. G.; Jang, J. A Novel Sensor Platform Based on Aptamer-Conjugated Polypyrrole Nanotubes for Label-Free Electrochemical Protein Detection. *ChemBioChem* **2008**, *9* (4), 634−641.
(37) Fang, Z.; Eshbaugh, A. A.; Schanze, K. S. Low-Bandgap Donor−Acceptor Conjugated Polymer Sensitizers for Dye-Sensitized Solar Cells. *J. Am. Chem. Soc.* **2011**, *133* (9), 3063−3069.
(38) Lee, K.; Cho, S.; Kim, M.; Kim, J.; Ryu, J.; Shin, K.-Y.; Jang, J. Highly Porous Nanostructured Polyaniline/Carbon Nanodots as Efficient Counter Electrodes for Pt-Free Dye-Sensitized Solar cells. *J. Mater. Chem. A* **2015**, *3* (37), 19018−19026.
(39) Shin, D. H.; Lee, J. S.; Jun, J.; Kim, S. G.; Jang, J. Detection of Hazardous Gas Using Multidemensional Porous Iron Oxide Nanorods-Decorated Carbon Nanoparticles. *ACS Appl. Mater. Interfaces* **2015**, *7* (3), 1746−1751.
(40) Cho, S.; Lee, J. S.; Jun, J.; Kim, S. G.; Jang, J. Fabrication of Water-Dispersible and Highly Conductive PSS-Doped PANI/Graphene Nanocomposites Using a High-Molecular Weight PSS Dopant and Their Application in H_2S Detection. *Nanoscale* **2014**, *6* (24), 15181−15195.
(41) Jun, J.; Lee, J. S.; Shin, D. H.; Kim, S. G.; Jang, J. Multidimensional MnO_2 Nanohair-Decorated Hybrid Multichannel Carbon Nanofiber as an Electrode Material for High-Performance Supercapacitors. *Nanoscale* **2015**, *7* (38), 16026−16033.
(42) Shin, D. H.; Lee, J. S.; Jun, J.; An, J. H.; Kim, S. G.; Cho, K. H.; Jang, J. Flower-like Palladium Nanoclusters Decorated Graphene Electrodes for Ultrasensitive and Flexible Hydrogen Gas Sensing. *Sci. Rep.* **2015**, *5*, 12294.
(43) Lee, J. S.; Oh, J.; Kim, S. G.; Jang, J. Highly Sensitive and Selective Field-Effect-Transistor Nonenzyme Dopamine Sensors Based on Pt/Conducting Polymer Hybrid Nanoparticles. *Small* **2015**, *11* (20), 2399−2406.
(44) Jun, J.; Lee, J. S.; Shin, D. H.; Jang, J. Aptamer-Functionalized Hybrid Carbon Nanofiber FET-Type Electrode for a Highly Sensitive

DOI: 10.1021/acsami.5b11159
ACS Appl. Mater. Interfaces XXXX, XXX, XXX−XXX

and Selective Platelet-Derived Growth Factor Biosensor. *ACS Appl. Mater. Interfaces* **2014**, *6* (16), 13859−13865.
(45) Feigel, I. M.; Vedala, H.; Star, A. Biosensors Based on One-Dimensional Nanostructures. *J. Mater. Chem.* **2011**, *21* (25), 8940−8954.
(46) Zhang, L.; Ding, Q.; Huang, Y.; Gu, H.; Miao, Y. E.; Liu, T. Flexible Hybrid Membranes with $Ni(OH)_2$ Nanoplatelets Vertically Grown on Electrospun Carbon Nanofibers for High-Performance Supercapacitors. *ACS Appl. Mater. Interfaces* **2015**, *7* (40), 22669−22677.
(47) Liao, J.-Y.; Higgins, D.; Lui, G.; Chabot, V.; Xiao, X.; Chen, Z. Multifunctional TiO_2−C/MnO_2 Core−Double-Shell Nanowire Arrays as High-Performance 3D Electrodes for Lithium Ion Batteries. *Nano Lett.* **2013**, *13* (11), 5467−5473.
(48) Qiu, Y.; Li, G.; Hou, Y.; Pan, Z.; Li, H.; Li, W.; Liu, M.; Ye, F.; Yang, X.; Zhang, Y. Vertically Aligned Carbon Nanotubes on Carbon Nanofibers: A Hierarchical Three-Dimensional Carbon Nanostructure for High-Energy Flexible Supercapacitors. *Chem. Mater.* **2015**, *27* (4), 1194−1200.
(49) Jung, C.-H.; Kim, W.-J.; Jung, C.-H.; Hwang, I.-T.; Khim, D.; Kim, D.-Y.; Lee, J.-S.; Ku, B.-C.; Choi, J.-H. A Simple PAN-Based Fabrication Method for Microstructured Carbon Electrodes for Organic Field-Effect Transistors. *Carbon* **2015**, *87*, 257−268.
(50) Georgakilas, V.; Perman, J. A.; Tucek, J.; Zboril, R. Broad Family of Carbon Nanoallotropes: Classification, Chemistry, and Applications of Fullerenes, Carbon Dots, Nanotubes, Graphene, Nanodiamonds, and Combined Superstructures. *Chem. Rev.* **2015**, *115* (11), 4744−4822.
(51) Li, D.; Xia, Y. Electrospinning of Nanofibers: Reinventing the Wheel? *Adv. Mater.* **2004**, *16* (14), 1151−1170.
(52) Zhang, Z.; Li, X.; Wang, C.; Wei, L.; Liu, Y.; Shao, C. ZnO Hollow Nanofibers: Fabrication from Facile Single Capillary Electrospinning and Applications in Gas Sensors. *J. Phys. Chem. C* **2009**, *113* (45), 19397−19403.
(53) Huang, Y.; Miao, Y.-E.; Ji, S.; Tjiu, W. W.; Liu, T. Electrospun Carbon Nanofibers Decorated with Ag−Pt Bimetallic Nanoparticles for Selective Detection of Dopamine. *ACS Appl. Mater. Interfaces* **2014**, *6* (15), 12449−12456.
(54) Kim, C.; Jeong, Y. I.; Ngoc, B. T. N.; Yang, K. S.; Kojima, M.; Kim, Y. A.; Endo, M.; Lee, J.-W. Synthesis and Characterization of Porous Carbon Nanofibers with Hollow Cores Through the Thermal Treatment of Electrospun Copolymeric Nanofiber Webs. *Small* **2007**, *3* (1), 91−95.
(55) Xin, X.; Sun, S.; Li, H.; Wang, M.; Jia, R. Electrochemical Bisphenol A Sensor Based on Core-Shell Multiwalled Carbon Nanotubes/Graphene Oxide Nanoribbons. *Sens. Actuators, B* **2015**, *209*, 275−280.
(56) Zehani, N.; Fortgang, P.; Saddek Lachgar, M.; Baraket, A.; Arab, M.; Dzyadevych, S. V.; Kherrat, R.; Jaffrezic-Renault, N. Highly Sensitive Electrochemical Biosensor for Bisphenol A Detection Based on a Diazonium-Functionalized Boron-Doped Diamond Electrode Modified with a Multi-Walled Carbon Nanotube-Tyrosinase Hybrid Film. *Biosens. Bioelectron.* **2015**, *74*, 830−835.
(57) Chen, L.; Zeng, X.; Ferhan, A. R.; Chi, Y.; Kim, D.-H.; Chen, G. Signal-On Electrochemiluminescent Aptasensors Based on Target Controlled Permeable Films. *Chem. Commun.* **2015**, *51* (6), 1035−1038.
(58) Chartuprayoon, N.; Zhang, M.; Bosze, W.; Choa, Y.-H.; Myung, N. V. One-Dimensional Nanostructures Based Bio-Detection. *Biosens. Bioelectron.* **2015**, *63*, 432−443.
(59) Yoon, H.; Lee, S. H.; Kwon, O. S.; Song, H. S.; Oh, E. H.; Park, T. H.; Jang, J. Polypyrrole Nanotubes Conjugated with Human Olfactory Receptors: High-Performance Transducers for FET-Type Bioelectronic Noses. *Angew. Chem., Int. Ed.* **2009**, *48* (15), 2755−2758.
(60) Lee, J. S.; Kim, S. G.; Jun, J.; Shin, D. H.; Jang, J. Aptamer-Functionalized Multidimensional Conducting-Polymer Nanoparticles for an Ultrasensitive and Selective Field-Effect-Transistor Endocrine-Disruptor Sensors. *Adv. Funct. Mater.* **2014**, *24* (39), 6145−6153.
(61) Hermann, T.; Patel, D. J. Adaptive Recognition by Nucleic Acid Aptamers. *Science* **2000**, *287* (5454), 820−825.
(62) Gao, Y.; Cao, Y.; Yang, D.; Luo, X.; Tang, Y.; Li, H. Sensitivity and Selectivity Determination of Bisphenol A Using SWCNT−CD Conjugate Modified Glassy Carbon Electrode. *J. Hazard. Mater.* **2012**, *199−200*, 111−118.
(63) Biedermann, S.; Tschudin, P.; Grob, K. Transfer of Bisphenol A from Thermal Printer Paper to the Skin. *Anal. Bioanal. Chem.* **2010**, *398* (1), 571−576.
(64) Mei, Z.; Chu, H.; Chen, W.; Xue, F.; Liu, J.; Xu, H.; Zhang, R.; Zheng, L. Ultrasensitive One-Step Rapid Visual Detection of Bisphenol A in Water Samples by Label-Free Aptasensor. *Biosens. Bioelectron.* **2013**, *39* (1), 26−30.
(65) Zhang, Y.; Cao, T.; Huang, X.; Liu, M.; Shi, H.; Zhao, G. A Visible-Light Driven Photoelectrochemical Aptasensor for Endocrine Disrupting Chemicals Bisphenol A with High Sensitivity and Specificity. *Electroanalysis* **2013**, *25* (7), 1787−1795.
(66) Wu, L.; Deng, D.; Jin, J.; Lu, X.; Chen, J. Nanographene-Based Tyrosinase Biosensor for Rapid Detection of Bisphenol A. *Biosens. Bioelectron.* **2012**, *35* (1), 193−199.
(67) Xue, F.; Wu, J.; Chu, H.; Mei, Z.; Ye, Y.; Liu, J.; Zhang, R.; Peng, C.; Zheng, L.; Chen, W. Electrochemical Aptasensor for the Determination of Bisphenol A in Drinking Water. *Microchim. Acta* **2013**, *180* (1), 109−115.
(68) Zhu, Y.; Zhou, C.; Yan, X.; Yan, Y.; Wang, Q. Aptamer-Functionalized Nanoporous Gold Film for High-Performance Direct Electrochemical Detection of Bisphenol A in Human Serum. *Anal. Chim. Acta* **2015**, *883*, 81−89.
(69) Yao, D.; Wen, G.; Jiang, Z. A Highly Sensitive and Selective Resonance Rayleigh Scattering Method for Bisphenol A Detection Based on the Aptamer-Nanogold Catalysis of the $HAuCl_4$-Vitamin C Particle Reaction. *RSC Adv.* **2013**, *3* (32), 13353−13356.

DOI: 10.1021/acsami.5b11159
ACS Appl. Mater. Interfaces XXXX, XXX, XXX−XXX